Closed-Form Green's Functions for Cylindrically Stratified Media

Çağatay Tokgöz, *Student Member, IEEE,* and Gülbin Dural, *Member, IEEE*

***Abstract*—A numerically efficient technique is developed to obtain the spatial-domain closed-form Green's functions of the electric and magnetic fields due to z- and ϕ-oriented electric and magnetic sources embedded in an arbitrary layer of a cylindrical stratified medium. First, the electric- and magnetic-field components representing the coupled TM and TE modes are derived in the spectral domain for an arbitrary observation layer. The spectral-domain Green's functions are then obtained and approximated in terms of complex exponentials in two consecutive steps by using the generalized pencil of function method. For the Green's functions approximated in the first step, the large argument behavior of the zeroth-order Hankel functions is used for the transformation into the spatial domain with the use of the Sommerfeld identity. In the second step, the remaining part of the Green's functions are approximated on two complementary parts of a proposed deformed path and transformed into the spatial domain, analytically. The results obtained in the two consecutive steps are combined to yield the spatial-domain Green's functions in closed forms.**

***Index Terms*—Closed forms, cylinders, cylindrical antennas, Green's function, Hankel transforms, nonhomogeneous media, spectral-domain analysis.**

I. Introduction

DUE TO THE advantages of microstrip antennas, such as their low weight, low cost, and flexibility, microstrip geometries mounted on layered structures have become very popular in various applications ranging from satellite and vehicular communications, and remote sensing to radiators in biomedical applications [1], [2].

Multilayer cylindrical structures can be used as practical models in a wide variety of applications. A typical example of such a modeling is the representation of a graded-index optical fiber with many piecewise homogeneous layers. Radar cross section for the scattering by the inlets of aircrafts can be reduced by coating the inlets with multilayer materials. Importance of cylindrically layered structures have led to the investigation of the scattering from conducting, dielectric, or dielectric-coated conducting cylinders, as well as the radiation from cylindrical–rectangular and wraparound microstrip and patch antennas [3]–[18].

Computation of the spatial-domain Green's functions requires a tedious and time-consuming numerical integration of the spectral-domain Green's functions, which are derived recursively for layered geometries. Therefore, the idea of closed-form spatial-domain Green's functions was proposed [19] and then extended to planarly layered structures [20]–[22] to avoid such an integration. In the analysis of spherically layered media, a significant amount of work has also been done and reported in [23]–[25].

There are a number of publications in which dispersion phenomena for the waves guided along a cylindrical stratified medium are presented [25]–[32]. Unlike those in planarly and spherically layered media, TM and TE waves are coupled together at an interface in cylindrically layered media. This requires simultaneous solution of the fields corresponding to TM and TE cases, the only exceptions being the rotationally symmetric $(n = 0)$ and z-invariant $(k_z = 0)$ cases for which separate analyses of TM and TE modes are possible. The coupled-mode analysis required for cylindrical structures results in reflection and transmission matrices rather than reflection and transmission coefficients. Some researchers have represented the reflection and transmission of waves at an interface between two adjacent cylindrical strata by 4×4 matrices in their publications [30], [31]. A simpler and less redundant algorithm using 2×2 matrices in field analysis has also been presented in [25] and [26], where only the z components of fields are used to represent the modes guided through layers.

Although several forms of Green's functions for multilayer cylindrical geometries are present in the literature [24], [25], [33], [34], closed-form expressions have not yet been reported in the spatial domain. The major contribution of this paper is to develop a two-step technique for obtaining the spatial-domain Green's functions in closed forms for a cylindrically layered medium, shown in Fig. 1. Closed-form expressions for the spectral-domain Green's functions of the electric and magnetic fields due to z- and ϕ-oriented electric and magnetic sources embedded in an arbitrary layer are derived for an arbitrary observation layer, analytically, by using a recursive algorithm for the coupled TM and TE modes. These Green's functions are sampled and approximated in two regions in terms of complex exponentials by using the generalized pencil of function (GPOF) method [35]. In the first region, where the large argument behavior of the zeroth-order Hankel functions enables complex exponentials of k_ρ to be represented in terms of Hankel functions, the Sommerfeld integral identity is used to transform Green's functions into the spatial domain. Hankel function representation obtained for this region is subtracted from the original Green's functions in the full domain, resulting in Green's functions vanishing outside a limited region. These Green's functions are then approximated in terms of complex exponentials

Manuscript received May 11, 1998.

Ç. Tokgöz was with the Department of Electrical and Electronics Engineering, Middle East Technical University, 06531 Ankara, Turkey. He is now with the ElectroScience Laboratory, Department of Electrical Engineering, The Ohio State University, Columbus, OH 43212 USA.

G. Dural is with the Department of Electrical and Electronics Engineering, Middle East Technical University, 06531 Ankara, Turkey.

Publisher Item Identifier S 0018-9480(00)00210-6.

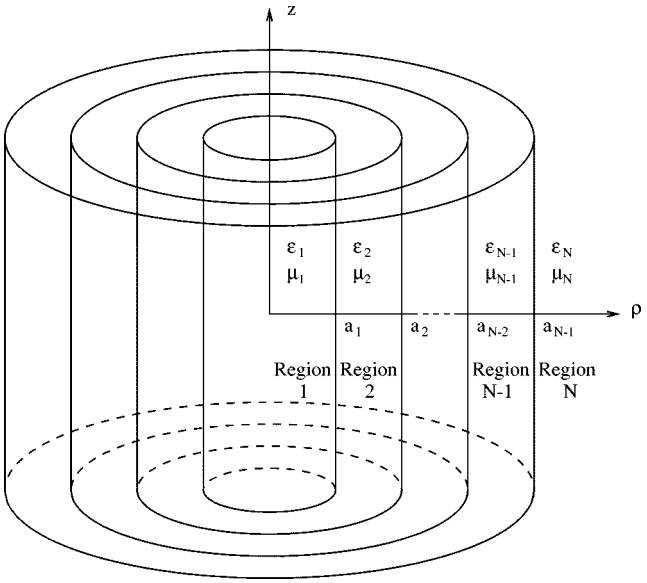

Fig. 1. Multiple interface geometry.

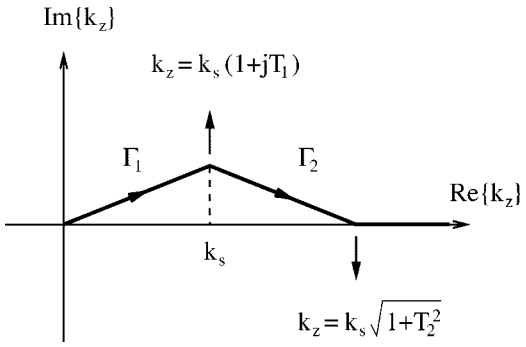

Fig. 2. Deformed path.

along the two contours Γ_1 and Γ_2 of a new path, which is shown in Fig. 2, and obtained by the deformation of the folded original integration path to avoid the branch-point singularity associated with a branch-cut and pole singularities encountered along the real axis on the complex k_z plane [36]. In this second region, transformation into the spatial domain turns out to be the analytical evaluation of two simple contour integrals of exponential functions. Finally, addition of the contributions of each step gives the spatial-domain Green's functions in closed forms.

II. Formulation

A cylindrical multilayer geometry is shown in Fig. 1. An electric or magnetic source can be embedded at (ρ', ϕ', z') in layer j and an observation point can be located at (ρ, ϕ, z) in an arbitrary layer i. Layers may vary in their electric and magnetic properties (ϵ_i, μ_i), as well as their thicknesses. Moreover, a perfect electric conductor (PEC) or perfect magnetic conductor (PMC) can be considered as the innermost or outermost layer. The following are the important steps carried out in the derivation of the closed-form Green's functions.

1) Derivation of the spectral-domain Green's functions.
   a) The z components of fields are derived for the coupled TM and TE modes in the source layer.
   b) These field components are then transferred, recursively, into the observation layer where Green's functions are obtained.
2) Derivation of the closed-form Green's functions in the spatial domain.
   a) Due to the pole singularities on the real axis and the branch-point singularities at $k_z = \mp k_N$ where k_N is the wavenumber of the outermost layer, the Sommerfeld integral is not integrable along the real axis on the complex k_z plane [25], [36]. Therefore, this original path is folded and deformed into the path shown in Fig. 2.
   b) Green's functions are sampled and approximated in terms of complex exponentials along the new path.
   c) The approximated Green's functions are transformed into the spatial domain in two steps, analytically.

The spectral-domain Green's functions are derived, recursively, following a similar procedure as in [25] and [37]. Hence, they are presented in Section II-A without giving the details of the derivation.

A. Green's Functions in the Spectral Domain

In general, a point electric or magnetic source of unit strength is represented by a current element

$$\vec{J}(\vec{r}) = \hat{\alpha}\delta\left(\vec{r} - \vec{r'}\right) \tag{1}$$

where $\hat{\alpha}$ is the unit vector in the current direction and it is assumed to be either $\hat{z}$ or $\hat{\phi}$ in the analysis, depending on whether a source of z or ϕ orientation is considered, respectively. The z components of the electric and magnetic fields can be written as a sum of the direct term due to the source, and the standing and outgoing waves which are, respectively, formed by the multiple reflections from the outer and inner boundaries of the source layer and represented by the first-kind Bessel and second-kind Hankel functions. Thus, the z components of the fields can be obtained in the source layer as

$$\begin{bmatrix} \tilde{E}_{z_n} \\ \tilde{H}_{z_n} \end{bmatrix} = \Big\{ J_n(k_{\rho_j}\rho_<) H_n^{(2)}(k_{\rho_j}\rho_>)\overline{I} + J_n(k_{\rho_j}\rho)\overline{A}_{n_s} + H_n^{(2)}(k_{\rho_j}\rho)\overline{A}_{n_o} \Big\} \overleftarrow{S}_n \tag{2}$$

where $\tilde{E}_{z_n}$ and $\tilde{H}_{z_n}$ represent the nth harmonics for the electric and magnetic fields, respectively, in the spectral domain. In (2), $\rho_<$ and $\rho_>$ are, respectively, the smaller and larger of ρ and ρ', and $\overleftarrow{S}_n$ is a 2 × 1 matrix operator that acts on functions to its left-hand side and is given by

$$\overleftarrow{S}_n = \begin{bmatrix} \frac{1}{\epsilon_j}\left(k_j^2 \hat{a}_z + jk_z\vec{\nabla}'\right)\cdot\hat{\alpha} \\ -jw\hat{\alpha}\cdot\left(\hat{a}_z \times \vec{\nabla}'\right) \end{bmatrix} \tag{3}$$

for the fields due to an electric source and

$$\overleftarrow{S}_n = \begin{bmatrix} jw\hat{\alpha}\cdot\left(\hat{a}_z\times\vec{\nabla}'\right) \\ \frac{1}{\mu_j}\left(k_j^2\hat{a}_z + jk_z\vec{\nabla}'\right)\cdot\hat{\alpha} \end{bmatrix} \tag{4}$$

for the fields due to a magnetic source.

Amplitudes for the nth harmonics of the reflected waves are represented by 2 × 2 matrices $\overline{A}_{n_s}$ and $\overline{A}_{n_o}$, which can be determined by applying the boundary conditions at the inner and outer interfaces of the source layer to yield

$$\begin{bmatrix} \tilde{E}_{z_n} \\ \tilde{H}_{z_n} \end{bmatrix} = \begin{cases} \left[J_n(k_{\rho_j}\rho)\overline{I} + H_n^{(2)}(k_{\rho_j}\rho)\tilde{\overline{R}}_{j,\,j-1}\right]\overline{A}_{n_j}, & \rho < \rho' \\ \left[H_n^{(2)}(k_{\rho_j}\rho)\overline{I} + J_n(k_{\rho_j}\rho)\tilde{\overline{R}}_{j,\,j+1}\right]\overline{A}_{n_j}, & \rho > \rho' \end{cases} \tag{5}$$

where $\overline{A}_{n_j}$ is a 2 × 1 amplitude matrix for the nth harmonic of the standing and outgoing waves for $\rho < \rho'$ and $\rho > \rho'$, respectively, in the source layer. The amplitudes of the standing waves in a layer different from the source layer are related to those in the adjacent layers by

$$\overline{A}_{n_{i-1}} = \left(\overline{I} - \overline{R}_{i-1,\,i}\tilde{\overline{R}}_{i-1,\,i-2}\right)^{-1}\overline{T}_{i,\,i-1}\overline{A}_{n_i} \tag{6}$$

where $\overline{A}_{n_{i-1}}$ and $\overline{A}_{n_i}$ are the amplitude matrices for the nth harmonics of the standing waves in layers $i-1$ and i, respectively. Similarly, the amplitudes of the outgoing waves can be related as

$$\overline{A}_{n_{i+1}} = \left(\overline{I} - \overline{R}_{i+1,\,i}\tilde{\overline{R}}_{i+1,\,i+2}\right)^{-1}\overline{T}_{i,\,i+1}\overline{A}_{n_i} \tag{7}$$

where $\overline{A}_{n_{i+1}}$ and $\overline{A}_{n_i}$ are the amplitude matrices for the nth harmonics of the outgoing waves in layers $i+1$ and i, respectively. $\overline{T}_{p,\,q}$, $\overline{R}_{p,\,q}$, and $\overline{R}_{p,\,q}$ are 2 × 2 local transmission, local reflection and generalized reflection matrices for the waves incident from layer p into layer q, respectively. Hence, the field expressions for any layer can be derived, iteratively, from those of the source layer [25], [37].

Depending on the field expressions of the observation layer, the spectral-domain Green's functions are derived as

$$\tilde{G}_{pq}^{E,\,H} = -\frac{1}{4w}\sum_{n=-\infty}^{\infty} e^{jn(\phi-\phi')}\tilde{G}_{pq}^{E_n,\,H_n} \tag{8}$$

where $\tilde{G}_{pq}^{E_n,\,H_n}$ is obtained for the z- and ϕ-oriented electric and magnetic sources as follows.

1) z-oriented electric dipole:

$$\tilde{G}_{zz}^{E_n} = \frac{k_{\rho_j}^2}{\epsilon_j}f_{11} \tag{9}$$

$$\frac{\tilde{G}_{zz}^{H_n}}{k_z} = \frac{k_{\rho_j}^2}{\epsilon_j}\frac{f_{21}}{k_z} \tag{10}$$

$$\frac{\tilde{G}_{\phi z}^{E_n}}{k_z} = \frac{k_{\rho_j}^2}{\epsilon_j}\left(\frac{n}{k_{\rho_i}^2\rho}f_{11} + \frac{jw\mu_i}{k_z k_{\rho_i}^2}\frac{\partial f_{21}}{\partial\rho}\right) \tag{11}$$

$$\tilde{G}_{\phi z}^{H_n} = \frac{k_{\rho_j}^2}{\epsilon_j}\left(-\frac{jw\epsilon_i}{k_{\rho_i}^2}\frac{\partial f_{11}}{\partial\rho} + \frac{nk_z}{k_{\rho_i}^2\rho}f_{21}\right). \tag{12}$$

2) ϕ-oriented electric dipole:

$$\frac{\tilde{G}_{z\phi}^{E_n}}{k_z} = \frac{n}{\epsilon_j\rho'}f_{11} - \frac{jw}{k_z}\frac{\partial f_{12}}{\partial\rho'} \tag{13}$$

$$\tilde{G}_{z\phi}^{H_n} = \frac{nk_z}{\epsilon_j\rho'}f_{21} - jw\frac{\partial f_{22}}{\partial\rho'} \tag{14}$$

$$\begin{aligned}\tilde{G}_{\phi\phi}^{E_n} =& \frac{nk_z}{\epsilon_j\rho'}\left(\frac{nk_z}{k_{\rho_i}^2\rho}f_{11} + \frac{jw\mu_i}{k_{\rho_i}^2}\frac{\partial f_{21}}{\partial\rho}\right) \\ &- jw\frac{\partial}{\partial\rho'}\left(\frac{nk_z}{k_{\rho_i}^2\rho}f_{12} + \frac{jw\mu_i}{k_{\rho_i}^2}\frac{\partial f_{22}}{\partial\rho}\right)\end{aligned} \tag{15}$$

$$\begin{aligned}\frac{\tilde{G}_{\phi\phi}^{H_n}}{k_z} =& \frac{n}{\epsilon_j\rho'}\left(-\frac{jw\epsilon_i}{k_{\rho_i}^2}\frac{\partial f_{11}}{\partial\rho} + \frac{nk_z}{k_{\rho_i}^2\rho}f_{21}\right) \\ &- jw\frac{\partial}{\partial\rho'}\left(-\frac{jw\epsilon_i}{k_z k_{\rho_i}^2}\frac{\partial f_{12}}{\partial\rho} + \frac{n}{k_{\rho_i}^2\rho}f_{22}\right)\end{aligned} \tag{16}$$

3) z-oriented magnetic dipole:

$$\frac{\tilde{G}_{zz}^{E_n}}{k_z} = \frac{k_{\rho_j}^2}{\mu_j}\frac{f_{12}}{k_z} \tag{17}$$

$$\tilde{G}_{zz}^{H_n} = \frac{k_{\rho_j}^2}{\mu_j}f_{22} \tag{18}$$

$$\tilde{G}_{\phi z}^{E_n} = \frac{k_{\rho_j}^2}{\mu_j}\left(\frac{nk_z}{k_{\rho_i}^2\rho}f_{12} + \frac{jw\mu_i}{k_{\rho_i}^2}\frac{\partial f_{22}}{\partial\rho}\right) \tag{19}$$

$$\frac{\tilde{G}_{\phi z}^{H_n}}{k_z} = \frac{k_{\rho_j}^2}{\mu_j}\left(-\frac{jw\epsilon_i}{k_z k_{\rho_i}^2}\frac{\partial f_{12}}{\partial\rho} + \frac{n}{k_{\rho_i}^2\rho}f_{22}\right) \tag{20}$$

4) ϕ-oriented magnetic dipole:

$$\tilde{G}_{z\phi}^{E_n} = jw\frac{\partial f_{11}}{\partial\rho'} + \frac{nk_z}{\mu_j\rho'}f_{12} \tag{21}$$

$$\frac{\tilde{G}_{z\phi}^{H_n}}{k_z} = \frac{jw}{k_z}\frac{\partial f_{21}}{\partial\rho'} + \frac{n}{\mu_j\rho'}f_{22} \tag{22}$$

$$\begin{aligned}\frac{\tilde{G}_{\phi\phi}^{E_n}}{k_z} =& jw\frac{\partial}{\partial\rho'}\left(\frac{n}{k_{\rho_i}^2\rho}f_{11} + \frac{jw\mu_i}{k_z k_{\rho_i}^2}\frac{\partial f_{21}}{\partial\rho}\right) \\ &+ \frac{n}{\mu_j\rho'}\left(\frac{nk_z}{k_{\rho_i}^2\rho}f_{12} + \frac{jw\mu_i}{k_{\rho_i}^2}\frac{\partial f_{22}}{\partial\rho}\right)\end{aligned} \tag{23}$$

$$\begin{aligned}\tilde{G}_{\phi\phi}^{H_n} =& jw\frac{\partial}{\partial\rho'}\left(-\frac{jw\epsilon_i}{k_{\rho_i}^2}\frac{\partial f_{11}}{\partial\rho} + \frac{nk_z}{k_{\rho_i}^2\rho}f_{21}\right) \\ &+ \frac{nk_z}{\mu_j\rho'}\left(-\frac{jw\epsilon_i}{k_{\rho_i}^2}\frac{\partial f_{12}}{\partial\rho} + \frac{nk_z}{k_{\rho_i}^2\rho}f_{22}\right)\end{aligned} \tag{24}$$

with

$$\overline{F}_n = \begin{cases} \left[J_n(k_{\rho_i}\rho)\overline{I} + H_n^{(2)}(k_{\rho_i}\rho)\tilde{\overline{R}}_{i,\,i-1}\right]\overline{A}_{n_i}, & \rho < \rho' \\ \left[H_n^{(2)}(k_{\rho_i}\rho)\overline{I} + J_n(k_{\rho_i}\rho)\tilde{\overline{R}}_{i,\,i+1}\right]\overline{A}_{n_i}, & \rho > \rho' \end{cases} = \begin{bmatrix} f_{11} & f_{12} \\ f_{21} & f_{22} \end{bmatrix}\overleftarrow{S}_n\,. \tag{25}$$

In (9)–(24), $\tilde{G}_{pq}^{E_n,H_n}$ denotes the nth harmonic of the spectral-domain Green's function for the electric and magnetic fields in direction p due to a unit q-oriented current element, $k_j^2 = k_z^2 + k_{\rho_j}^2$, $k_i^2 = k_z^2 + k_{\rho_i}^2$, the subscripts j and i indicate the source and observation layers, and the superscripts E and H represent the electric and magnetic fields, respectively.

Note that, in (10), (11), (13), (16), (17), (20), (22), and (23), $\tilde{G}_{pq}^{E_n,H_n}/k_z$ is given instead of $\tilde{G}_{pq}^{E_n,H_n}$ itself to represent the Green's functions as even functions of k_z for the proper use in the approximation procedure explained in Section II-B. Since the division by k_z corresponds to integration with respect to k_z in the spatial domain, the integral of the spatial-domain Green's function is approximated from which the spatial-domain Green's function itself can easily be obtained [21], [22].

B. Closed-Form Green's Functions in the Spatial Domain

The spectral-domain Green's functions can be transformed into the spatial domain by

$$G(z-z') = \frac{1}{2\pi}\int_{-\infty}^{\infty} dk_z e^{-jk_z(z-z')}\tilde{G}(k_z) \tag{26}$$

where G is the spatial-domain Green's functions and $\tilde{G}$ is either $\tilde{G}_{pq}^{E,H}$ or $\tilde{G}_{pq}^{E,H}/k_z$ depending on whether $\tilde{G}_{pq}^{E,H}$ is an even or odd function of k_z, respectively. Since $\tilde{G}$ is chosen to be an even function of k_z, the inverse Fourier integral (26) can be folded as

$$G(z-z') = \frac{1}{\pi}\int_0^{\infty} dk_z \cos\Big[k_z(z-z')\Big]\tilde{G}(k_z). \tag{27}$$

Along the original path of integration, branch-point singularities at $k_z = \mp k_N$ and pole singularities are encountered, k_N being the wavenumber of the outermost layer [25], [36]. Due to these singularities, the inverse Fourier integral (26) is not integrable along the real axis on the complex k_z plane in a lossless medium. Therefore, a new path obtained by the deformation of the folded original integration path, and shown in Fig. 2, is introduced to avoid the pole and branch-point singularities. The spectral-domain Green's functions are sampled and approximated in terms of complex exponentials on this deformed path using the GPOF method and then transformed into the spatial domain by applying a two-step approximation technique outlined as follows [22].

1) Transformation by the Sommerfeld identity using the large argument behavior of the zeroth-order Hankel functions.
   a) The spectral-domain Green's functions are sampled uniformly along the path

$$\left.\begin{aligned} k_{\rho_s} &= -jk_s(t_3+T_2) \\ k_z &= k_s\sqrt{1+(t_3+T_2)^2} \end{aligned}\right\} 0 \le t_3 < T_3 - T_2 \tag{28}$$

   where k_s and k_{ρ_s} are the wavenumbers of the sampling region that is chosen as the source layer. With this step, the original integration path is mapped into an equivalent path in the k_ρ plane.
   b) The value of T_2 should be large enough to avoid the pole and branch-point singularities and in order for the large argument approximation of the zeroth-order Hankel functions to be valid. Hence, a choice of T_2 such that $k_s\sqrt{1+T_2^2}$ is greater than the wavenumbers of all layers should be appropriate. Once T_2 is chosen, the value of $T_3 \cong 1.1T_2$ is sufficient to capture the behavior of the Green's functions in the sampling interval.
   c) The sampled Green's functions are multiplied by $\sqrt{k_{\rho_s}}$ and approximated in terms of N_3 complex exponentials of k_{ρ_s} by the GPOF method as

$$\sqrt{k_{\rho_s}}\tilde{G}_{k_\rho} \cong \sum_{\ell=1}^{N_3} b_{\ell_t} e^{s_{\ell_t}t_3} = \sum_{\ell=1}^{N_3} b_{\ell_k} e^{k_{\rho_s}s_{\ell_k}} \tag{29}$$

   where $\tilde{G}_{k_\rho}$ represents the spectral-domain Green's functions approximated in this region.
   d) The resulting exponential functions are represented by the zeroth-order Hankel functions using the large argument approximation as

$$\tilde{G}_{k_\rho} \cong \sum_{\ell=1}^{N_3} b_{\ell_k}\frac{e^{k_{\rho_s}s_{\ell_k}}}{\sqrt{k_{\rho_s}}} \cong \sum_{\ell=1}^{N_3} b_{\ell_h} H_0^{(2)}(k_{\rho_s}s_{\ell_h}). \tag{30}$$

   e) Then, by using the Sommerfeld identity

$$\frac{e^{-jk_s|\vec{r}-\vec{r}'|}}{|\vec{r}-\vec{r}'|} = -j\int_0^{\infty} dk_z \cos\Big[k_z(z-z')\Big]H_0^{(2)}\Big(k_{\rho_s}|\vec{\rho}-\vec{\rho}'|\Big) \tag{31}$$

   where $|\vec{r}-\vec{r}'| = \sqrt{(z-z')^2+|\vec{\rho}-\vec{\rho}'|^2}$, the spatial-domain Green's functions G_{k_ρ} are obtained as

$$G_{k_\rho} \cong \frac{j}{\pi}\sum_{\ell=1}^{N_3} b_{\ell_h}\frac{e^{-jk_s|r_\ell|}}{|r_\ell|} \tag{32}$$

   where $r_\ell = \sqrt{(z-z')^2+s_{\ell_h}^2}$.

2) Analytical transformation.
   a) The spectral-domain Green's functions $\tilde{G}_{k_\rho}$ approximated in the first step are subtracted from the original Green's functions $\tilde{G}$ to yield the Green's functions $\tilde{G}_{k_z}$ vanishing for $k_z \ge k_s\sqrt{1+T_2^2}$.
   b) The resulting Green's functions $\tilde{G}_{k_z}$ are sampled uniformly along the two contours Γ_1 and Γ_2, which are shown in Fig. 2 and given, respectively, as

$$k_z = k_s(1+jT_1)\frac{t_1}{T_1}, \qquad 0 \le t_1 < T_1 \tag{33}$$

   and

$$k_z = k_s\left[1+jT_1+\left(\sqrt{1+T_2^2}-1-jT_1\right)\frac{t_2}{T_2-T_1}\right], \qquad 0 \le t_2 < T_2 - T_1. \tag{34}$$

   c) Along the paths (33) and (34), the imaginary part of k_z has a maximum value of k_sT_1 at $t_1 = T_1$ and $t_2 = 0$, respectively, where maximum deviation from the original path occurs. Therefore, the deformation of the path can be controlled by choosing T_1 properly. This parameter should be sufficiently large to overcome the effects of the pole and branch-point singularities and small enough to avoid numerical difficulties. For a robust and safe approximation, T_1 should be so chosen that $k_sT_1 \cong 0.1k_0$, where k_0 is the wavenumber of free space.

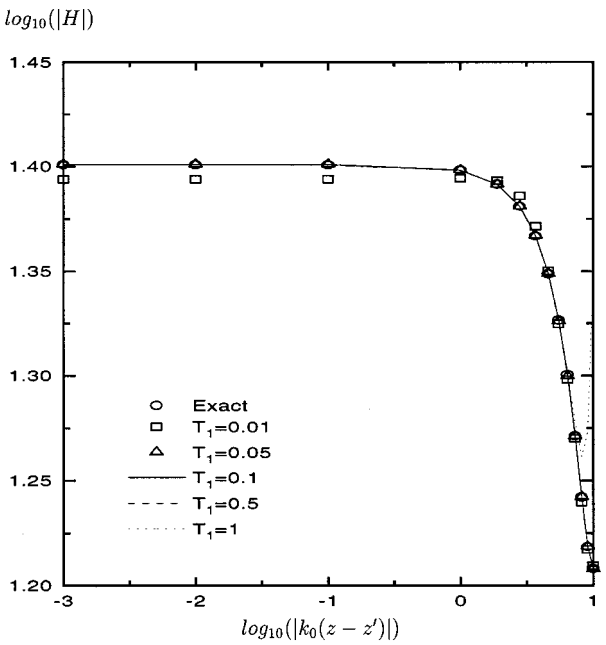

Fig. 3. $\log_{10}(|H|)$ for $\bar{H} = \sum_{k=1}^{3} a_k H_0^{(2)}(k_\rho \rho_k)$. $k = 59.2788$, $a_1 = 3.86$, $a_2 = 7.13$, $a_3 = 2.95$, $\rho_1 = 0.42$, $\rho_2 = 0.25$, $\rho_3 = 0.58$.

d) The sampled Green's functions are approximated in terms of N_1 and N_2 complex exponentials of k_z by the GPOF method, respectively, on the paths (33) and (34) as

$$\tilde{G}_{k_z} \cong \sum_{m=1}^{N_1} b_{m_t} e^{s_{m_t} t_1} + \sum_{n=1}^{N_2} b_{n_t} e^{s_{n_t} t_2} \cong \sum_{m=1}^{N_1} b_{m_k} e^{k_z s_{m_k}} + \sum_{n=1}^{N_2} b_{n_k} e^{k_z s_{n_k}}. \quad (35)$$

e) Transformation of the approximated Green's functions into the spatial domain turns out to be a simple contour integral of exponential functions as

$$G_{k_z} = \frac{1}{\pi} \int_{\Gamma_1 + \Gamma_2} dk_z \cos\left[k_z(z - z')\right] \tilde{G}_{k_z}. \quad (36)$$

Addition of the contributions of the two steps yields the spatial-domain Green's functions in closed forms.

III. Numerical Results and Discussions

In this paper, a numerically efficient technique is developed to represent Green's functions in closed forms. The spectral-domain Green's functions are sampled on a path obtained by folding and deforming the original Sommerfeld integration path. This deformed path should be constructed by choosing the deformation parameters T_1, T_2, and T_3, appropriately. The value of T_1 should be sufficiently large to overcome the effects of the pole and branch-point singularities on sampling. On the other hand, it should be chosen small enough to avoid numerical difficulties. Moreover, the value of T_2 should be large enough so that $k_s\sqrt{1+T_2^2}$ is greater than the wavenumbers of all layers to ensure that the deformed path does not pass through any one of the pole and branch-point singularities and the large argument approximation of the zeroth-order Hankel functions

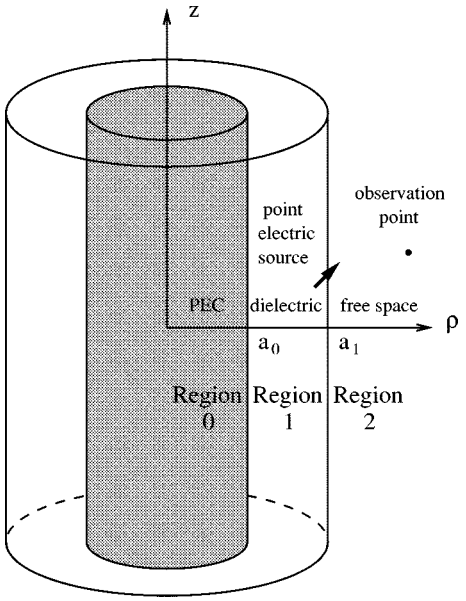

Fig. 4. Dielectric-coated conducting cylinder. Region 0: PEC. Region 1: $\epsilon_{r_1} = 2.3$, $\mu_{r_1} = 1$. Region 2: free space, $a_0 = 20$ mm, $a_1 = \rho' = 21$ mm, $\rho = 40$ mm, $\phi - \phi' = \pi/6$ rad, $f = 4.7$ GHz.

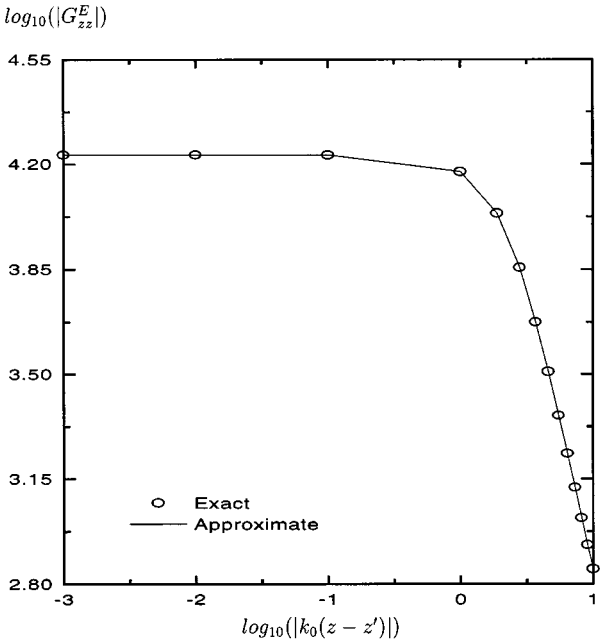

Fig. 5. Magnitude of the Green's function G_{zz}^E. Region 0: PEC. Region 1: $\epsilon_{r_1} = 2.3$, $\mu_{r_1} = 1$. Region 2: free space, $a_0 = 20$ mm, $a_1 = \rho' = 21$ mm, $\rho = 40$ mm, $\phi - \phi' = \pi/6$ rad, $f = 4.7$ GHz.

can be used. Once the value of T_2 is determined, T_3 can be safely chosen around $1.1T_2$. A total number of approximately 200 samples can be sufficient for sampling in the spectral domain to obtain satisfactory results in the spatial domain.

To investigate the effect of path deformation on the approximation procedure, a function formed as a sum of three Hankel functions in the spectral domain is sampled on a deformed path for several values of T_1 and transformed into the spatial domain in closed forms for each value of T_1 individually. The results obtained by these transformations are compared with those computed by the analytical transformation using the Sommerfeld

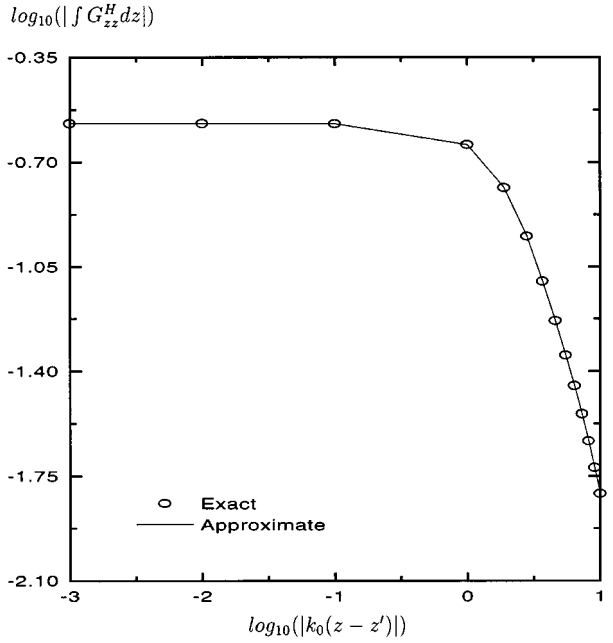

Fig. 6. Magnitude of the Green's function $\int G^H_{zz} dz$. Region 0: PEC. Region 1: $\epsilon_{r_1} = 2.3, \mu_{r_1} = 1$. Region 2: free space, $a_0 = 20$ mm, $a_1 = \rho' = 21$ mm, $\rho = 40$ mm, $\phi - \phi' = \pi/6$ rad, $f = 4.7$ GHz.

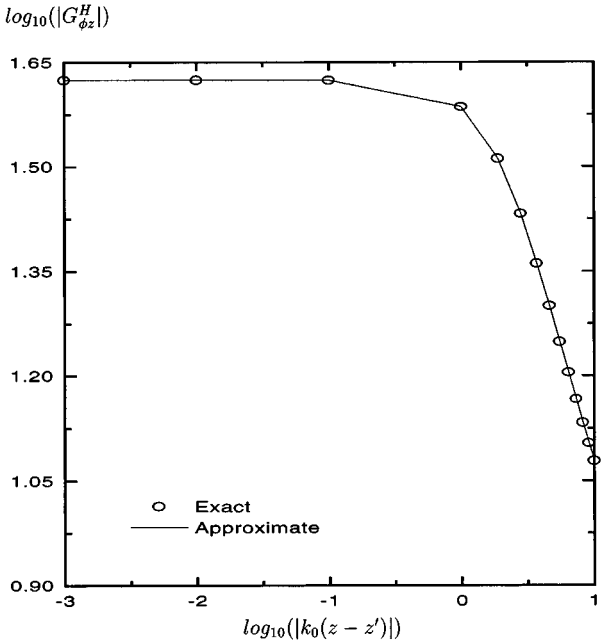

Fig. 8. Magnitude of the Green's function $G^H_{\phi z}$. Region 0: PEC, Region 1: $\epsilon_{r_1} = 2.3, \mu_{r_1} = 1$. Region 2: free space, $a_0 = 20$ mm, $a_1 = \rho' = 21$ mm, $\rho = 40$ mm, $\phi - \phi' = \pi/6$ rad, $f = 4.7$ GHz.

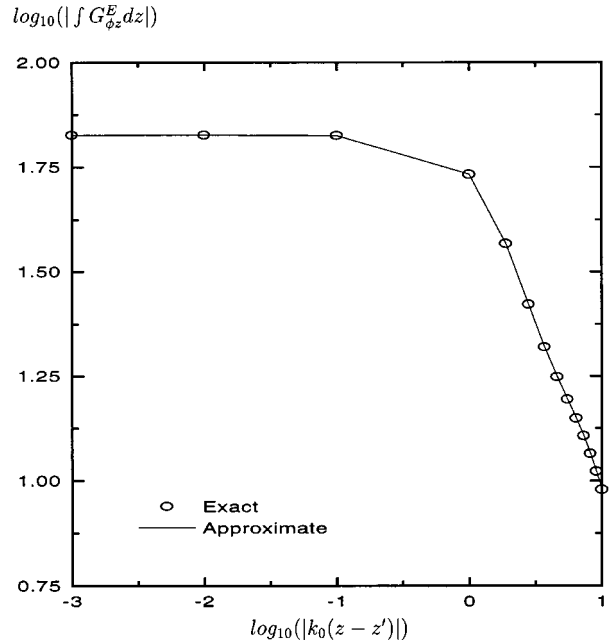

Fig. 7. Magnitude of the Green's function $\int G^E_{\phi z} dz$. Region 0: PEC. Region 1: $\epsilon_{r_1} = 2.3, \mu_{r_1} = 1$. Region 2: free space, $a_0 = 20$ mm, $a_1 = \rho' = 21$ mm, $\rho = 40$ mm, $\phi - \phi' = \pi/6$ rad, $f = 4.7$ GHz.

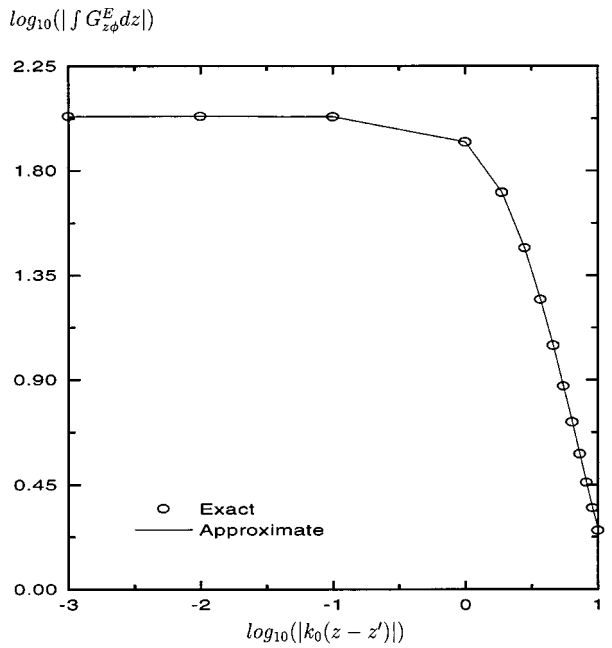

Fig. 9. Magnitude of the Green's function $\int G^E_{z\phi} dz$. Region 0: PEC. Region 1: $\epsilon_{r_1} = 2.3, \mu_{r_1} = 1$. Region 2: free space, $a_0 = 20$ mm, $a_1 = \rho' = 21$ mm, $\rho = 40$ mm, $\phi - \phi' = \pi/6$ rad, $f = 4.7$ GHz.

identity. It is observed in Fig. 3 that $T_1 = 0.01$ is too small and $T_1 = 1$ is too large to provide a good approximation on the deformed path, which deviates too much from the original path. The other approximate results obtained for the values of $T_1 = 0.05, T_1 = 0.1$, and $T_1 = 0.5$ are in good agreement with the exact values, as shown in Fig. 3. Experiences on numerical computations indicate that $k_s T_1$, which is the maximum deviation from the original path, should be around $0.1k_0$ for a robust and safe approximation.

In this section, layered cylindrical geometries with various source excitations are also investigated. Approximate results obtained by the closed-form approximation technique are compared with the exact values computed by the numerical evaluation of the inverse Fourier integral (27).

The Green's functions that are divided by k_z in the spectral domain to obtain even functions of k_z are given as $|\int G^{E,H}_{pq} dz|$ rather than $|G^{E,H}_{pq}|$ in the spatial domain. These Green's functions can be recovered by operating the derivative $\partial/\partial z$ on

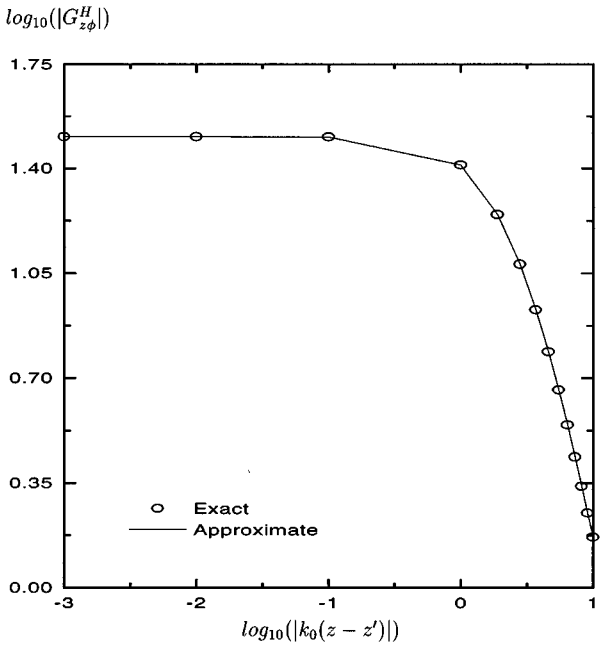

Fig. 10. Magnitude of the Green's function $G^H_{z\phi}$. Region 0: PEC. Region 1: $\epsilon_{r_1} = 2.3, \mu_{r_1} = 1$. Region 2: free space, $a_0 = 20$ mm, $a_1 = \rho' = 21$ mm, $\rho = 40$ mm, $\phi - \phi' = \pi/6$ rad, $f = 4.7$ GHz.

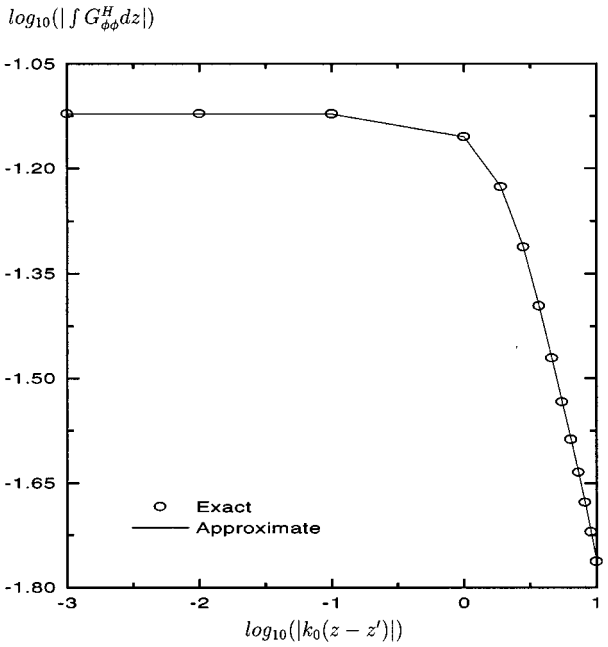

Fig. 12. Magnitude of the Green's function $\int G^H_{\phi\phi} dz$. Region 0: PEC. Region 1: $\epsilon_{r_1} = 2.3, \mu_{r_1} = 1$. Region 2: free space, $a_0 = 20$ mm, $a_1 = \rho' = 21$ mm, $\rho = 40$ mm, $\phi - \phi' = \pi/6$ rad, $f = 4.7$ GHz.

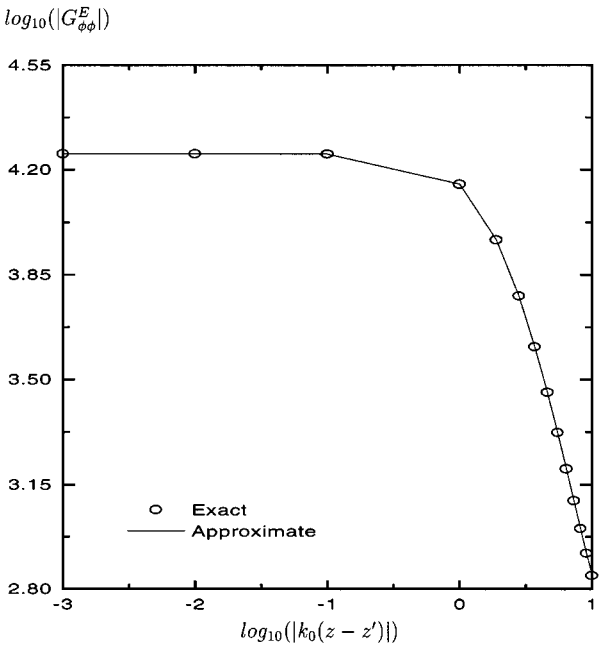

Fig. 11. Magnitude of the Green's function $G^E_{\phi\phi}$. Region 0: PEC. Region 1: $\epsilon_{r_1} = 2.3, \mu_{r_1} = 1$. Region 2: free space, $a_0 = 20$ mm, $a_1 = \rho' = 21$ mm, $\rho = 40$ mm, $\phi - \phi' = \pi/6$ rad, $f = 4.7$ GHz.

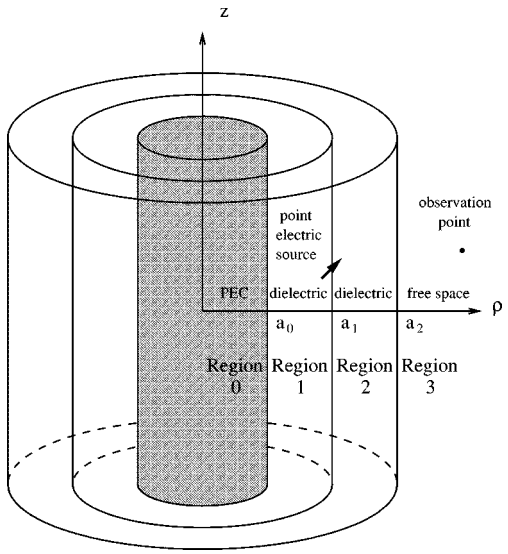

Fig. 13. Dielectric-coated conducting cylinder with a superstrate. Region 0: PEC. Region 1: $\epsilon_{r_1} = 2.3, \mu_{r_1} = 1$. Region 2: $\epsilon_{r_2} = 4, \mu_{r_2} = 1$. Region 3: free space $a_0 = 50$ mm, $a_1 = \rho' = 51$ mm, $a_2 = 52$ mm, $\rho = 70$ mm, $\phi - \phi' = \pi/6$ rad, $f = 6.8$ GHz.

them. In the method-of-moments applications, this derivative can be alternatively operated on expansion functions.

As the first example, a dielectric-coated conducting cylinder with a point electric source at the interface between the dielectric material and free space is investigated and modeled as a multilayer structure with the parameters: Region 0: PEC, Region 1: $\epsilon_{r_1} = 2.3$, $\mu_{r_1} = 1$, Region 2: free space, $a_0 = 20$ mm, $a_1 = \rho' = 21$ mm, $\rho = 40$ mm, $\phi - \phi' = \pi/6$rad at $f = 4.7$ GHz, as shown in Fig. 4. It is observed that the spectral-domain Green's functions of the electric field are in good agreement with those given in [7] for this geometry. The exact and approximate results for the spatial-domain Green's functions are consistent with each other, as shown in Figs. 5–12.

The second example geometry consists of a dielectric-coated conducting cylinder with a superstrate, as shown in Fig. 13,

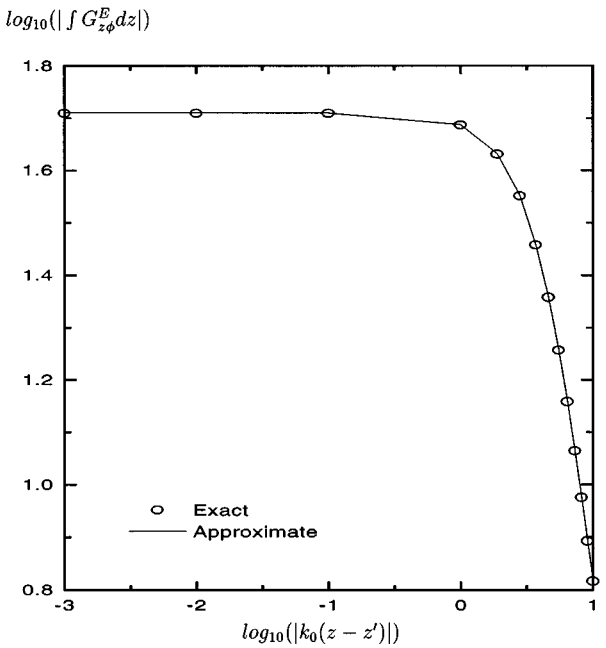

Fig. 14. Magnitude of the Green's function $\int G^E_{z\phi}dz$. Region 0: PEC. Region 1: $\epsilon_{r_1} = 2.3$, $\mu_{r_1} = 1$. Region 2: $\epsilon_{r_2} = 4$, $\mu_{r_2} = 1$. Region 3: free space, $a_0 = 50$ mm, $a_1 = \rho' = 51$ mm, $a_2 = 52$ mm, $\rho = 70$ mm, $\phi - \phi' = \pi/6$ rad, $f = 6.8$ GHz.

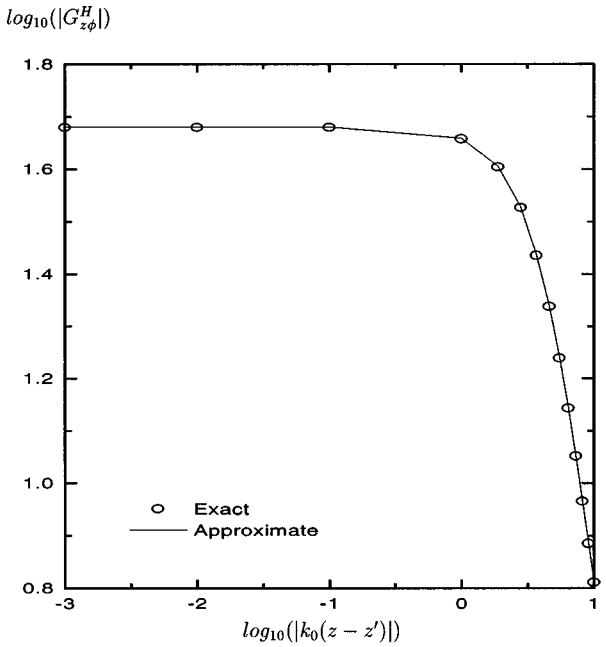

Fig. 15. Magnitude of the Green's function $G^H_{z\phi}$. Region 0: PEC. Region 1: $\epsilon_{r_1} = 2.3$, $\mu_{r_1} = 1$. Region 2: $\epsilon_{r_2} = 4$, $\mu_{r_2} = 1$. Region 3: free space, $a_0 = 50$ mm, $a_1 = \rho' = 51$ mm, $a_2 = 52$ mm, $\rho = 70$ mm, $\phi - \phi' = \pi/6$ rad, $f = 6.8$ GHz.

which has the parameters: Region 0: PEC, Region 1: $\epsilon_{r_1} = 2.3$, $\mu_{r_1} = 1$, Region 2: $\epsilon_{r_2} = 4$, $\mu_{r_2} = 1$, Region 3: free spaces $a_0 = 50$ mm, $a_1 = \rho' = 51$ mm, $a_2 = 52$ mm, $\rho = 70$ mm, $\phi - \phi' = \pi/6$rad. The geometry is excited by a ϕ-oriented point electric source at $f = 6.8$ GHz. The spatial-domain Green's functions are shown in Figs. 14–17.

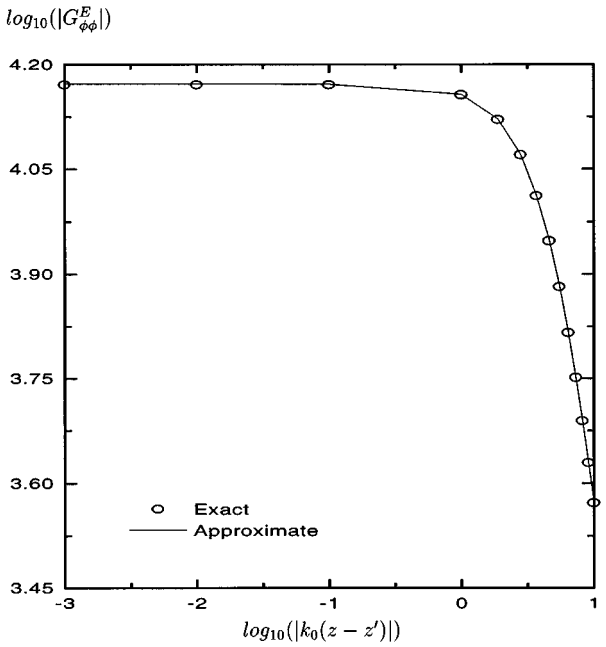

Fig. 16. Magnitude of the Green's function $G^E_{\phi\phi}$. Region 0: PEC. Region 1: $\epsilon_{r_1} = 2.3$, $\mu_{r_1} = 1$. Region 2: $\epsilon_{r_2} = 4$, $\mu_{r_2} = 1$. Region 3: free space, $a_0 = 50$ mm, $a_1 = \rho' = 51$ mm, $a_2 = 52$ mm, $\rho = 70$ mm, $\phi - \phi' = \pi/6$ rad, $f = 6.8$ GHz.

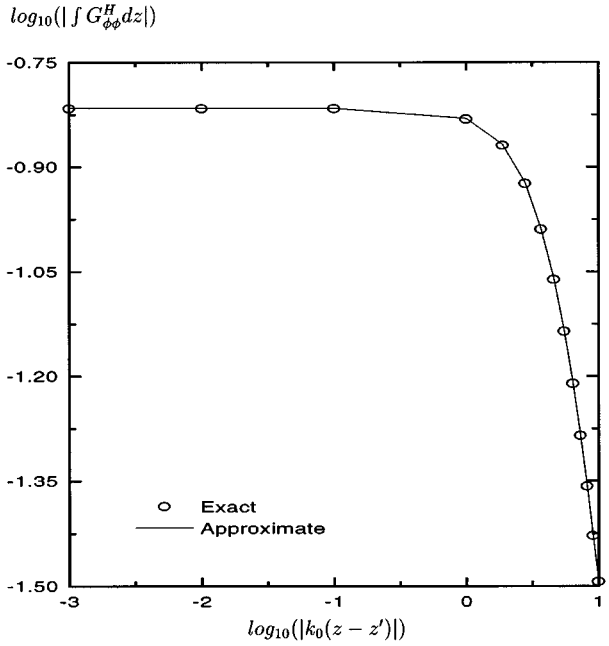

Fig. 17. Magnitude of the Green's function $\int G^H_{\phi\phi}dz$. Region 0: PEC. Region 1: $\epsilon_{r_1} = 2.3$, $\mu_{r_1} = 1$. Region 2: $\epsilon_{r_2} = 4$, $\mu_{r_2} = 1$. Region 3: free space, $a_0 = 50$ mm, $a_1 = \rho' = 51$ mm, $a_2 = 52$ mm, $\rho = 70$ mm, $\phi - \phi' = \pi/6$ rad, $f = 6.8$ GHz.

If the source and observation layers are the same, the direct term in (2) can be transformed into the spatial domain in closed form by using the Sommerfeld identity, and the approximation technique should be applied to the remaining terms. In the analysis by the method of moments, expansion and testing functions can be properly chosen and the approximation technique may be modified to improve the computational efficiency [21], [38].

The numerical examples presented in this section show that the approximation technique yields accurate results in the analysis of cylindrical structures. Therefore, this technique can be conveniently used to improve the computational efficiency in the numerical approach to the problems involving multilayer cylindrical geometries.

IV. Conclusion

A numerically efficient technique is developed to obtain closed-form spatial-domain Green's functions in an arbitrary layer for the electric and magnetic fields due to the electric and magnetic sources embedded in an arbitrary layer of a cylindrically stratified medium. This technique is based on the approximation of the spectral-domain Green's functions in terms of complex exponentials in two steps, where the large argument behavior of the zeroth-order Hankel functions is used for the transformation using the Sommerfeld identity in the first step and a simple contour integration is applied in the second step. The approximate results obtained by the use of the technique in the analysis of multilayer geometries are compared with the exact values computed by the numerical evaluation of the folded inverse Fourier integral (27). These results are found to be in good agreement.

Acknowledgment

The authors thank Prof. M. I. Aksun for the useful comments.

References

[1] K. R. Carver and J. W. Mink, "Microstrip antenna technology," *IEEE Trans. Antennas Propagat.*, vol. AP-29, pp. 2–24, Jan. 1981.

[2] R. E. Munson, "Conformal microstrip antennas and microstrip phased arrays," *IEEE Trans. Antennas Propagat.*, vol. AP-22, pp. 74–78, Jan. 1974.

[3] H. E. Bussey and J. H. Richmond, "Scattering by a lossy dielectric circular cylindrical multilayer, numerical values," *IEEE Trans. Antennas Propagat.*, vol. AP-23, pp. 723–725, Sept. 1975.

[4] L. C. Kempel and J. L. Volakis, "Scattering by cavity-backed antennas on a circular cylinder," *IEEE Trans. Antennas Propagat.*, vol. AP-42, pp. 1268–1279, Sept. 1994.

[5] L. C. Kempel, J. L. Volakis, and R. J. Sliva, "Radiation by cavity-backed antennas on a circular cylinder," *Proc. Inst. Elect. Eng.*, vol. 142, pp. 233–239, June 1995.

[6] J. Ashkenazy, S. Shtrikman, and D. Treves, "Electric surface current model for the analysis of microstrip antennas on cylindrical bodies," *IEEE Trans. Antennas Propagat.*, vol. AP-33, pp. 295–300, Mar. 1985.

[7] N. G. Alexopoulos and A. Nakatani, "Cylindrical substrate microstrip line characterization," *IEEE Trans. Microwave Theory Tech.*, vol. MTT-35, pp. 843–849, Sept. 1987.

[8] C. M. Krowne, "Cylindrical-rectangular microstrip antenna," *IEEE Trans. Antennas Propagat.*, vol. AP-31, pp. 194–199, Jan. 1983.

[9] K. M. Luk, K. F. Lee, and J. S. Dahele, "Analysis of cylindrical-rectangular patch antenna," *IEEE Trans. Antennas Propagat.*, vol. AP-37, pp. 143–147, Feb. 1989.

[10] K. M. Luk and K. F. Lee, "Characteristics of the cylindrical-circular patch antenna," *IEEE Trans. Antennas Propagat.*, vol. AP-38, pp. 1119–1123, July 1990.

[11] W. Y. Tam, A. K. Y. Lai, and K. M. Luk, "Cylindrical rectangular microstrip antennas with coplanar parasitic patches," in *Proc. Inst. Elect. Eng.*, vol. 142, Aug. 1995, pp. 300–306.

[12] J. F. Kiang, "Resonance properties of cylindrical rectangular patch with composite ground plane," in *Proc. Inst. Elect. Eng.*, vol. 142, Aug. 1995, pp. 307–313.

[13] K. L. Wong, Y. T. Cheng, and J. S. Row, "Resonance in a superstrate-loaded cylindrical-rectangular microstrip structure," *IEEE Trans. Microwave Theory Tech.*, vol. MTT-41, pp. 814–819, May 1993.

[14] R. B. Tsai and K. L. Wong, "Characterization of cylindrical microstriplines mounted inside a ground cylindrical surface," *IEEE Trans. Microwave Theory Tech.*, vol. MTT-43, pp. 1607–1610, July 1995.

[15] S. M. Ali, T. M. Habashy, J. F. Kiang, and J. A. Kong, "Resonance in cylindrical-rectangular and wraparound microstrip structures," *IEEE Trans. Microwave Theory Tech.*, vol. 37, pp. 1773–1783, Nov. 1989.

[16] T. M. Habashy, S. M. Ali, and J. A. Kong, "Input impedance and radiation pattern of cylindrical-rectangular and wraparound microstrip antennas," *IEEE Trans. Antennas Propagat.*, vol. 38, pp. 722–731, May 1990.

[17] S. B. A. Fonseca and A. J. Giarola, "Analysis of microstrip wraparound antennas using dyadic Green's functions," *IEEE Trans. Antennas Propagat.*, vol. AP-31, pp. 248–253, Mar. 1983.

[18] F. C. Silva, S. B. A. Fonseca, A. J. M. Soares, and A. J. Giarola, "Analysis of microstrip antennas on circular-cylindrical substrates with a dielectric overlay," *IEEE Trans. Antennas Propagat.*, vol. 39, pp. 1398–1404, Sept. 1991.

[19] Y. L. Chow, J. J. Yang, D. F. Fang, and G. E. Howard, "A closed-form spatial Green's function for the thick microstrip substrate," *IEEE Trans. Microwave Theory Tech.*, vol. 39, pp. 588–592, Mar. 1991.

[20] M. I. Aksun and R. Mittra, "Derivation of closed-form Green's functions for a general microstrip geometry," *IEEE Trans. Microwave Theory Tech.*, vol. 40, pp. 2055–2062, Nov. 1992.

[21] G. Dural and M. I. Aksun, "Closed-form Green's functions for general sources and stratified media," *IEEE Trans. Microwave Theory Tech.*, vol. 43, pp. 1545–1552, July 1995.

[22] M. I. Aksun, "A robust approach for the derivation of closed-form Green's functions," *IEEE Trans. Microwave Theory Tech.*, vol. 44, pp. 651–658, May 1996.

[23] L. W. Li, P. S. Kooi, M. S. Leong, and T. S. Yeo, "Electromagnetic dyadic Green's function in spherically multilayered media," *IEEE Trans. Microwave Theory Tech.*, vol. 42, pp. 2302–2310, Dec. 1994.

[24] C. T. Tai, *Dyadic Green's Functions in Electromagnetic Theory*, 2nd ed, New York: IEEE, 1993.

[25] W. C. Chew, *Waves and Fields in Inhomogeneous Media*, New York: Van Nostrand, 1990.

[26] J. R. Lovell and W. C. Chew, "Response of a point source in a multicylindrically layered medium," *IEEE Trans. Geosci. Remote Sensing*, vol. GRS-25, pp. 850–858, Nov. 1987.

[27] J. R. Wait, *Electromagnetic Propagation from Cylindrical Structures*, New York: Pergamon, 1959.

[28] L. B. Felsen and N. Marcuwitz, *Radiation and Scattering of Waves*. Englewood Cliffs, NJ: Prentice-Hall, 1973.

[29] L. B. Felsen and K. Naishadham, "Ray formulation of waves guided by circular cylindrically stratified dielectrics," *Radio Sci.*, vol. 26, pp. 203–209, 1991.

[30] K. Naishadham and L. B. Felsen, "Dispersion of waves guided along a cylindrical substrate-superstrate layered medium," *IEEE Trans. Antennas Propagat.*, vol. 41, pp. 304–313, Mar. 1993.

[31] L. W. Pearson, "A construction of the fields radiated by z-directed point sources of current in the presence of a cylindrically layered obstacle," *Radio Sci.*, vol. 21, pp. 559–569, 1986.

[32] J. A. Kong, *Electromagnetic Wave Theory*, New York: Wiley, 1990.

[33] S. B. A. Fonseca and A. J. Giarola, "Dyadic Green's functions and their use in the analysis of microstrip antennas," in *Advances in Electronics and Electron Physics*, New York: Academic, 1985, vol. 65, pp. 1–90.

[34] Z. Xiang and Y. Lu, "Electromagnetic dyadic Green's function in cylindrically multilayered media," *IEEE Trans. Microwave Theory Tech.*, vol. 44, pp. 614–621, Apr. 1996.

[35] Y. Hua and T. K. Sarkar, "Generalized pencil-of-function method for extracting poles of an EM system from its transient response," *IEEE Trans. Antennas Propagat.*, vol. 37, pp. 229–234, Feb. 1989.

[36] W. C. Chew, "The singularities of a Fourier-type integral in a multicylindrical layer problem," *IEEE Trans. Antennas Propagat.*, vol. AP-31, pp. 653–655, July 1983.

[37] Ç. Tokgöz, "Derivation of closed-form Green's functions for cylindrically stratified media," M.S. thesis, Dept. Elect. Electron. Eng., Middle East Technical Univ., Ankara, Turkey, Aug. 1997.

[38] M. I. Aksun and R. Mittra, "Choices of expansion and testing functions for the method of moments applied to a class of electromagnetic problems," *IEEE Trans. Microwave Theory Tech.*, vol. 41, pp. 503–509, Mar. 1993.

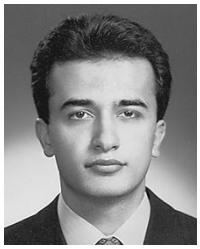

Çağatay Tokgöz (S'99) received the B.S. degree from Bilkent University, Ankara, Turkey, in 1994, and the M.S. degree from the Middle East Technical University, Ankara, Turkey, in 1997, both in electrical and electronics engineering, and is currently working toward the Ph.D. degree at The Ohio State University, Columbus.

From 1994 to 1996, he was with Aselsan Military Electronics Inc., Ankara, Turkey, as an RF Design Engineer. From 1996 to 1997, he was with the Middle East Technical University, as a Graduate Assistant. Since 1997, he has been a Graduate Research Associate in the ElectroScience Laboratory, The Ohio State University. His research interests include numerical methods and high-frequency asymptotic techniques for analysis of cylindrical structures.

Gülbin Dural (S'85–M'88) received the B.S. and M.S. degrees in electrical and electronics engineering from the Middle East Technical University, Ankara, Turkey, in 1981 and 1983, respectively, and the Ph.D. degree in electrical engineering from The Ohio State University, Columbus, in 1988.

From 1981 to 1983, she was a Graduate Assistant at the Middle East Technical University. From 1984 to 1988, she was a Graduate Research Associate with The Ohio State University ElectroScience Laboratory. Since 1989, she has been a faculty member of the Department of Electrical and Electronics Engineering, Middle East Technical University, where she is currently an Associate Professor. Her research interests include numerical methods for electromagnetics, microstrip antennas, microwave and millimeter-wave integrated circuits, and SAR and ISAR imaging techniques.